NATIONAL ADVISORY COMMITTEE FOR AERONAUTICS

TECHNICAL MEMORANDUM 1240

AIRFOIL MEASUREMENTS IN THE DVL HIGH-SPEED

WIND TUNNEL (2.7-METER DIAMETER)

By B. Göthert

Translation of "Profilmessungen im DVL-Hochgeschwindigkeitswindkanal (2,7-meter Durchmesser)." Lilienthal-Gesellschaft für Luftfahrtforschung, Bericht 156

NACA

Washington

June 1949

NATIONAL ADVISORY COMMITTEE FOR AERONAUTICS

TECHNICAL MEMORANDUM 1240

AIRFOIL MEASUREMENTS IN THE DVL HIGH-SPEED

WIND TUNNEL (2.7-METER DIAMETER)*

By B. Göthert

SUMMARY

The present report is a brief summary of the investigations on symmetrical and cambered airfoils in the DVL high-speed wind tunnel. In the light of measurements of wings of different aspect ratio with equal profile it is shown that the effect of the aspect ratio on the increase in lift with rising Mach number expected on the basis of calculations is closely confirmed by the measurements. Several recent experiments on a wing with the small aspect ratio of $b^2/F = 1.15$ are discussed, where the lift disclosed no disturbances within the test range, that is, up to angles of attack of $\alpha = 8°$ and Mach numbers of $M = 0.9$, and the drag (at $c_a = 0$) starts to increase at a much higher Mach number than for a wing with the same profile but greater aspect ratio.

I. INTRODUCTION

The airfoils tested in the DVL high-speed tunnel are represented in figure 1.[1] The tests primarily involved a series of symmetrical

---

*"Profilmessungen im DVL-Hochgeschwindigkeitswindkanal (2,7-meter Durchmesser)." Lilienthal-Gesellschaft für Luftfahrtforschung, Bericht 156, pp. 5-16.

[1]The notation for the profile used in figure 1, which is normal practice in the DVL, is exemplified on the NACA airfoil 1 30 12 - 1.1 40:

Depth of camber, percent . . . . f/l = 1
Distance of maximum camber from the leading edge,
  percent . . . . x_f/l = 30
Thickness ratio, percent . . . . d/l = 12
Nose radius, percent . . . . $\dfrac{p/l}{(d/l)^2}$ = 1.1

Backward position of maximum thickness from the nose,
  percent . . . . x_d/l = 40

The added letters NACA indicate that the contour of the NACA systemiga-tion is maintained.

standard NACA airfoils with thickness ratios ranging between
$d/l = 0.06$ and $d/l = 0.18$ (reference 1). In addition three
symmetrical profiles having thickness ratios of 9, 12, and 15 percent
with maximum thickness moved backward were investigated; the tests,
however, have not yet been correlated because of their use for
different purposes and the long delay between tests (reference 2).
So far only one profile with 2-percent camber and normal thickness
distribution has been investigated at the request of the Messer-
schmitt Co. (reference 3). A greater number of profiles of various
camber are ready to be tested. (In the meantime three more cambered
profiles were investigated up to January 1943.)

On the previously enumerated profiles the pressure distribution
was measured in the center section of the rectangular wings fitted
with end plates and the drag was computed from measurements of
momentum loss behind the model wings. The wing chord of all these
models was 500 and 350 millimeters, respectively, so that the
Reynolds number even at the lowest Mach number of the tests,
$(M = 0.30)$, with $Re_{min} \approx 2.2 \times 10^6$ was still considerably above
the critical value for the boundary-layer reversal on flat plates.

In addition a number of profiles with thickness ratio up to
$d/l = 0.50$ and chords of $l = 60$ millimeters and less were tested so
as to obtain a preliminary insight into the effects of such profiles
on the drag at high Mach numbers, especially with respect to
propellers.

II. RESULTS OF TESTS ON PROFILES AT HIGH SUBSONIC SPEEDS

1. Lift of Symmetrical Profiles

The value $\partial c_a/\partial \alpha$ governing the lift at high airspeeds was
determined for symmetrical profiles of varying thickness from DVL
tests and plotted against the Mach number in figure 2. The
theoretical curve for the lift increase according to Prandtl's
approximation ratio $1/\sqrt{1 - M^2}$, is included for comparison. In
the pure subsonic range, that is, up to the critical Mach
number, M^*, at which the velocity of sound is reached or exceeded locally,
the test curves of thin profiles up to $d/l = 12$ percent manifest
an increase in the $\partial c_a/\partial \alpha$ value which is in good agreement with
Prandtl's calculations. Only on the thickest profile with
$d/l = 18$ percent does the lift increase disappear with rising
Mach number, obviously as the result of the more unfavorable
development of the boundary layer on thick profiles.

After exceeding the critical Mach number M^*, that is, as soon as the sonic velocity is locally exceeded at the profile and compressibility shock occurs, the premises of the Prandtl law are no longer complied with, hence no agreement is to be expected between the experimental and theoretical curve. While in this range the lift increase for thin profiles up to $d/l = 12$ percent increases at first, and then shows no marked decrease until after substantially exceeding the critical Mach number, the lift on the thick profiles of $d/l = 15$ percent and 18 percent decreases as soon as the critical Mach number is exceeded and finally drops to zero at about $M = 0.83$. This dissimilar behavior of the lift on thin and thick profiles in the supercritical range of Mach numbers can be explained from the pressure-distribution records by the dissimilar development of the compressibility shocks.

On studying the range of Mach numbers on a profile with compressibility shock occurring only on the suction side (fig. 3), it is seen that this shock has already moved much farther toward the trailing edge on the thin profile than on the thick profile; this causes the earlier manifested lift increase on the thin profile and the lift decrease on the thick profile, as seen by a comparison with the pressure distribution curve at small Mach number indicated by thin lines.

If at further rise in Mach number the pressure side also happens to come into the range of the compressibility shock (fig. 4), these shocks develop on suction and pressure side near the trailing edge of thin profiles at sufficiently high subsonic Mach numbers, so that a large lifting surface remains, which however is substantially less compared to the pressure distribution without pressure-side compressibility shock. On the thick profile, on the other hand, the suction-side compressibility shock lags behind in its rearward movement, so that for the lifting surface at the forward part of the profile there is a corresponding negative lifting surface at the rear part of the profile and the lift therefore drops to zero or even negative values in spite of the positive angle of attack of the profile.

The formation of the cited pressure distributions also affords a possibility of estimating the lift distribution on profiles at higher Mach numbers than correspond to the measured range. As the pressure distribution of the thin profile in figure 4 indicates, at $M = 0.88$ the compressibility shocks on suction and pressure side have already travelled close to the trailing edge so that on this profile no further fundamental change in lift is to be expected. This is readily seen by a comparison with the pressure distribution of an airfoil at a supersonic speed, as represented in figure 5 according to a measurement by Ferri (reference 4). The pressure distribution

at supersonic velocity resembles in the low-pressure variation as
well as in the position of the compressibility shock the pressure
distribution on the thin profile. Accordingly it is to be presumed
that the curves for the lift increase in figure 2 may not be
extrapolated to zero for the thin profiles, but that the lift is
actually maintained throughout even at further approach to sonic
velocity. Several tests in the DVL high-speed tunnel are available
which show that the lift at the very high Mach number of M = 0.90
does not continue to drop steeply but rather starts again to rise
to higher lift coefficients. For the same reason it is to be
expected that on the thick airfoils a rise in Mach number beyond
the test range will be accompanied by a lift increase to rational
values, because the suction-side compressibility shock will travel
to the trailing edge even on the thick airfoils at sufficiently high
subsonic Mach numbers and so cancel the overlap in the pressure-
distribution plots.

2. Lift of Cambered Airfoils

Only one cambered airfoil with 2-percent depth of camber and
13-percent thickness ratio has been tested, although a large
number of cambered model wings had been prepared for testing.
Aside from the lift increase $\partial c_a/\partial \alpha$ and the drag which are
similar to those on symmetrical airfoils of equal thickness ratio,
an unusual result of these measurements was the sudden displacement
of the angle of attack for zero lift at high Mach numbers (fig. 6).
While up to M = 0.8 the angle for zero lift of the cambered airfoil
was located at $\alpha_0 = -1.5^\circ$, it rose to $\alpha_0 = 2^\circ$, or changed by
about 3.5° when the Mach number increased to M = 0.86. Thus
a wing must be given a 3.5° higher setting in this range, if lift
conditions similar to those at small Mach numbers are to be reached.
This displacement of zero angle of attack is also attributable to
a particular formation on the pressure side of the compressibility
shock that suddenly moves in direction of the wing trailing edge
in the 0.8 to 0.86 Mach number range (figs. 7 and 8).

3. Neutral Stability Point of Symmetrical Profiles

The neutral stability point which owing to the symmetry of the
profile in this instance also indicates the position of the applied
moment was computed for the series of NACA airfoils of varying thick-
ness from the pressure-distribution measurements over a range of
small lift coefficients. According to figure 9 the curves for the
varyingly thick profiles are so staggered at small and medium velocities
that for thick profiles the neutral stability point lies nearer to

the leading edge. This is due to the boundary layer which thickens
more on the suction than on the pressure side and therefore reduces the
lift at the trailing edge in accord with the effective jet boundary
at the edge of the boundary layer. This decrease in lift caused
by the one-sided thickening of the boundary layer is naturally
so much greater as the profile is thicker.

At increasing Mach number all neutral-point curves shift toward
the wing leading edge, the shift being greater for the thicker profiles.
This also is explainable by means of the boundary layer, since with
rising Mach number the pressures governing the boundary-layer
development increase and thus the same effect is produced as by a
further thickening of the profile.

After exceeding the critical Mach number, that is, after locally
exceeding the velocity of sound the curves of the thin airfoils with
6 to 12-percent thickness ratio bend sharply in direction of the
tail-heavy neutral stability-point positions, while the curves of the
thick profiles continue to rise in the old direction. This dissimilar
behavior in the range of the compressibility shocks is already evident
from the previously discussed pressure-distribution curves in this
speed range (figs. 3 and 4). Owing to the dissimilar compressibility-
shock position on the pressure and suction side of thick airfoils
it results in overlap in the pressure distribution which as a result
of the downwash shifts the applied moment forward. This overlap
cancels out on the thin airfoils especially at high Mach numbers.
On the contrary, the pressure distributions disclose that the applied
moment travels in direction of the wing center as in pure subsonic
flow.

4. Drag of Symmetrical Profiles

The drag of the symmetrical profiles with different thickness
ratios explored in the high-speed tunnel is plotted against the
Mach number in figure 10 for symmetrical air flow. There is no
change in drag coefficient up to the critical Mach number, that is,
in the subsonic range, but after a certain increase in Mach number
beyond the critical, the well known steep-drag rise occurs. The
amount of the drag rise covered on an average by these tests is up
to drag coefficients (referred to frontal area) of around 0.4.

In the pure subsonic range the drag coefficient of the profiles
tested is practically constant, although the Reynolds number of the
tests increases with increasing Mach number. This observation was
made on the symmetrical NACA airfoils as well as on other tests on
different models. In the evaluation of these curves

it should be remembered that the Reynolds number effect leading to
a drag decrement is opposed by the effect of compressibility on
increasing the velocities which acts in the sense of a drag increase.
Calculations for predicting the drag curve at subcritical Mach numbers
have up to the present not given the complete equality of these two
mutually counteracting influences; it must not be forgotten that these
approximation processes considered only the Reynolds number and
the apparently increased profile thickness, but not the compressi-
bility in the formation of the boundary layer. By this omission no
provision is made, for example, for the fact that substantial
temperature differences occur within the boundary layer which, for
instance, at the point where locally the velocity of sound is
exactly reached, already amounts to about 45° C. So when the
boundary-layer laws obtained for incompressible flow are applied
to compressible flow the difference between measurement and
preliminary calculation is, in view of this omitted temperature
gradient, not surprising.

Incidental to the steep drag increase the question arises as to
what values the drag will attain at further increasing Mach number.
From numerous measurements in the high-speed tunnel it was found
that the drag coefficient based on frontal area appears to tend
toward a terminal value of the order of magnitude of $c_w = 1.2$ at
high Mach numbers, so that this value may serve as reference point
for an extrapolation of the drag coefficients beyond the test range.

This value is confirmed satisfactorily by the measurements on
thick symmetrical airfoils of small chord represented in figure 11,
and whose thickness ratio had been raised to 50 percent in view of
propeller root profiles. The profile chord of these wings ranged
between 36 and 60 millimeters, the span was about 500 millimeters.
The wings were mounted on an adjustable central spindle, the drag
at zero setting was determined by means of a thin wire extending
forward at the model. These measurements also show within measuring
accuracy the nearly constant drag coefficient up to the critical
Mach number.

III. CORRELATION OF THE PROFILE MEASUREMENTS IN THE

DVL HIGH-SPEED TUNNEL WITH THE MEASUREMENTS IN THE

LARGE WIND TUNNEL OF THE DVL

The measurements in the DVL high-speed tunnel generally cover a
speed range of from 100 meters per second to about 90 percent of the

velocity of sound. At the lowest airspeed compressibility usually has such a small effect that the test data in this range are directly comparable with the measurements in low-speed wind tunnels.

The series of symmetrical NACA airfoil sections, for which an abstract from the high-speed measurement is given in the present report, was also tested in the large tunnel of the DVL (5 × 7 meters) at low speeds (reference 5). The data from both tests are compared in figures 12 and 14. For the comparison the tests from the high-speed tunnel were extrapolated to the Mach number of $M = 0.2$ corresponding to the speed in the large tunnel which involved no difficulties in view of the flatness of the curves in this range of Mach numbers. The Reynolds number in both wind-tunnel tests was $Re \approx 2.7 \times 10^6$. The agreement between the measurements in both tunnels is unusually good. The discrepancies in drag and in moment about the quarter-chord point range within measuring accuracy.

Only for the lift increase $\partial c_a / \partial \alpha$ do the high-speed measurements systematically exceed those of the large tunnel by about 5 percent. This difference is probably due to the fact that normal wings with aspect ratio $b^2/F = 5$ were used in the large tunnel, while the wings in the high-speed tunnel were fitted with end plates. In the conversion of the angle of attack with the end-plate measurements to two-dimensional flow, it is conceivable that the simple equations employed for taking the end plate into account, according to O. Schrenk, still contain certain inaccuracies.

IV. EFFECT OF ASPECT RATIO ON THE AERODYNAMIC

COEFFICIENTS OF RECTANGULAR WINGS

The previously reported test data were obtained, as a rule, from pressure-distribution measurements in the center section of rectangular wings, hence reproduce the profile characteristics for two-dimensional flow in good approximation. The drag measurements on the small wings of large thickness with their comparatively large aspect ratios, $b^2/F \approx 10$ or more, form the only exception.

1. Effect of Aspect Ratio

In the pure subsonic range it is of importance to know whether the aspect ratio acts in accord with the theoretical calculations (reference 6) on the rise in the lift increase $\partial c_a / \partial \alpha$ with increasing Mach number. According to these calculations the lift

increases at constant angle of attack of the wing only in two-dimensional flow in the ratio $1/\sqrt{1 - M^2}$, while for finite aspect ratio the rise is smaller and disappears altogether in the extreme case of very small aspect ratios.

On the basis of later measurements on wings with the same profile NACA 00012 - 1.130 with three different aspect ratios ($b^2/F = \infty$ from pressure-distribution measurements, and $b^2/F = 6$ and 1.15 from force measurements) this question regarding the lift increase could be answered to the extent that the test data are in satisfactory agreement with the calculations. On the wing with very small aspect ratio in particular, $b^2/F = 1.15$, the rise of the $\partial c_a/\partial \alpha$ values with increasing Mach number is extremely small (fig. 15).

According to the cited theoretical investigations this diminished rise in $\partial c_a/\partial \alpha$ for small aspect ratio is attributable to the fact that, while the lift belonging to the effective angle of attack of the wing increases in accord with the calculations for two-dimensional flow with the Prandtl factor $1/\sqrt{1 - M^2}$, the induced downwash angle at the wing also increases as a result of the increased lift and so reduces the lift by way of the effective angle of attack. This reduced lift increase is therefore so much greater as the downwash effect is greater, that is, as the aspect ratio becomes smaller. For the very same reason this reduction disappears completely when as for infinite aspect ratio the downwash is infinitely small.

The measurements for $b^2/F = \infty$ and $b^2/F = 6$ show no substantial differences in their fundamental distribution even in the supercritical range of Mach numbers, as for instance, the temporary marked rise in lift after exceeding the velocity of sound followed by a marked drop as a result of the pressure-distribution overlap. On the wing with aspect ratio $b^2/F = 6$, which was measured up to $M \approx 0.90$, it is noted again that the lift characteristic $\partial c_a/\partial \alpha$ at very high Mach numbers of $M = 0.90$ no longer decreases but begins to rise again with further increase in Mach number.

From this general trend for $b^2/F \rightarrow \infty$ and $b^2/F = 6$ the test curve of the wing with $b^2/F = 1.15$ differs in noticeable manner, to the extent that this wing neither exhibits a greater increase nor a marked decrease in the $\partial c_a/\partial \alpha$ curve in the supercritical range of Mach numbers.

2. Wing With Aspect Ratio $b^2/F = 1.15$

(NACA airfoil section 00012 - 1.130)[2]

The wing designed with the NACA airfoil section 00012 - 1.130
had a chord of $l = 0.35$ meters. It was supported at wing center
by a single balance support which transmitted the lift and drag of the
model wing at a 45° angle obliquely to the balance. The moment was
measured on a separate balance over a symmetrical moment arm.

Lift: Figure 16 shows the lift coefficient c_a plotted against
the angle of attack α for several Mach numbers. In contrast to all
profile measurements known so far, no disturbances of any kind were
observed throughout the entire range of Mach numbers up to $M = 0.91$,
notwithstanding the fact that the angle of attack was raised up to
$\alpha = 8^{\circ}$, save that the highest Mach number $M = 0.91$ at high α
no longer yields the slight deflection of the lift curve in direction
of higher c_a, but on the contrary, a slight deflection in the
opposite sense, that is, toward lower c_a. However, it is to be
noted that the lift coefficient as a result of the small aspect ratio
at $\alpha = 8^{\circ}$ mounts to little more than $c_a = 0.2$.

Schlieren observations made contemporary with the force measure-
ments indicated that at $M = 0.82$ severe compressibility shocks
occurred even at zero angle of attack. According to the Schlieren
photographs the location of the compressibility shocks on the
pressure side was a little nearer to the trailing edge than on the
suction side, so that the overlap observed on the profile in
two-dimensional flow and the loss in lift produced by it, was
largely canceled out.

The small effect of the Mach number on the rise of the lift curves
$c_a = f(\alpha)$ is more accurately represented in figure 17 on the variation
of the lift increase $\partial c_a/\partial \alpha$ with respect to the Mach number.
$\partial c_a/\partial \alpha$ increases very little, in fact, a little less even than the
theory stipulates.

Moment: In figure 18 the moment coefficient referred to the
$l/4$ chord of the wings is plotted against the lift coefficient c_a
for several Mach numbers. According to it the moment curves are
not rectilinear any more even at low speeds, and this oscillating
variation is considerably simplified at increasing Mach number.

---

[2]These measurements are to be published as a separate report
in the near future.

But discontinuous moment jumps as on wings in two-dimensional
flow are completely absent.

Another unusual fact is that the moment curves with rising
Mach number turn considerably in the unstable sense, which
corresponds to a shift of the neutral stability point toward the
leading edge (fig. 19). Even at low speeds the neutral stability
point, which owing to the symmetrical wing profile is also
identical with the center of pressure, lies about 18 percent
ahead of the $l/4$ point, that is, only about 7 percent aft of
the wing leading edge. This forward position is explained by the
fact that owing to the small aspect ratio of the wing, the stream
lines are considerably curved compared to the wing chord which at
the tip especially leads to greater negative lift and even loss
of lift. Since at high Mach numbers for the model wing with
$b^2/F = 1.15$ there corresponds a comparable wing in incompressible
flow with a smaller aspect ratio, the further forward shift of
the neutral stability point with increasing Mach number is readily
understood, even though the magnitude of this travel was, at first,
surprising. For example, the neutral point lies already at the nose
when $M = 0.76$ is reached; at still higher M it and with it the
center of pressure lies even ahead of the wing leading edge.

A comparison with Winter's tests on wings of small aspect
ratios (reference 7) indicated that a wing with $b^2/F \approx 1$ and
12.7-percent thickness ratio corresponding to the previously
reported measurements likewise exhibited a very forwardly located
neutral stability point, which was determined as being less than
10 percent behind the leading edge.

Drag: The drag of the wing with $b^2/F = 1.15$ in symmetrical
flow is plotted against the Mach number in figure 20, along with
the corresponding drag curves of the rectangular wing with $b^2/F = 6$
and of a wing with 35° positive sweepback and $b^2/F = 6$. All wings
had the same NACA 00012 - 1.130 profile. The drag increase on the
wing with $b^2/F = 1.15$ is considerably delayed relative to the
rectangular wing and starts only a little earlier than on the wing
with 35° positive angle of sweepback. The reduction from $b^2/F = 6$
to $b^2/F = 1.15$ therefore causes the same delay in drag increase
at high Mach numbers, as obtained for $b^2/F = 6$ with a 30° positive
sweepback.

The cause of this beneficial drag action of the wing with small
aspect ratio is likely to be found in a transition to three-
dimensional flow as a result of the small aspect ratio. At the
wing tips, whose range of influence in this particular case amounts
to a considerable portion of the total wing area, a flow occurs which

is rather comparable to an axially symmetrical than to a two-dimensional flow, and as a consequence exhibits the more favorable characteristics of a three-dimensional flow.

V. RECAPITULATION

1. A brief survey of the airfoil measurements in the DVL high-speed tunnel is given in the light of several diagrams.

2. By measurements on wings of different aspect ratios it is proved that in the pure subsonic range the aspect ratio affects the rise of the lift as the theory stipulates. Thus the lift for wings of infinite aspect ratio, for example, increases with $1/\sqrt{1 - M^2}$, while in the extreme case of vanishingly small aspect ratio the lift remains constant in spite of increasing Mach number.

3. High-speed measurements on a rectangular wing with $b^2/F = 1.15$ disclosed that in the entire test range, that is, up to $M = 0.90$ and angles of attack up to $\alpha = 8^\circ$, no rough discontinuities in lift and moment were observed. The drag rise at zero lift on this wing compared to the wing of $b^2/F = 6$ was shifted considerably toward higher Mach numbers.

DISCUSSION

Knappe: Göthert's drag curves showed no rise at small and medium Mach numbers. But according to theoretical considerations a linear increase above the Prandtl factor should occur, as definitely observed in the Heinkel tunnel. The reason that this effect did not occur on Göthert's curves might be found in a superposition of mutually opposing effects of Reynolds and Mach number. In the measurements in the Heinkel high-speed tunnel the effect of the Reynolds number was suppressed by "turbulence edges." This is also plainly observed on the position of the test points on part of Göthert's curves.

Helmbold. According to Göthert (JB. 1941, DLF, p. I, 684) it is possible to correct the airspeed in the tunnel, even when supersonic areas already occur at the profile. Promise is, of course, that they do not yet reach the tunnel wall. But this condition exists long before reaching the velocity of sound. In this respect the free jet shows more favorable characteristics, since on it the supersonic areas extending out from the profile

are able to reach the jet boundary only when the jet leaves the
nozzle with sonic velocity. The corrective possibility which
in the tunnel rests on the measurement of the minimum pressure
at maximum speed at the tunnel wall and provides reference points
for the prediction of the intensity of the reflected dipole grid
by means of the Prandtl-Busemann law is, on the free jet, given
by the measurement of the greatest jet expansion and the subsequent
determination of the reflected dipole grid. The correction possi-
bility therefore ends only at sonic velocity on the free jet.

Translated by J. Vanier
National Advisory Committee
for Aeronautics

REFERENCES

1. Göthert, B.:   Profilmessungen im DVL-Hochgeschwindigkeitswindkanal
      (2,7 m ∅). FB 1490.

   Göthert, B.:   Druckverteilungs- und Impulsverlustschaubilder für
      das Profil NACA 0 00 06 - 1,1 30 bei hohen Unterschallgeschwin-
      digkeiten. FB 1505/1.

   FB 1505/2:   dasselbe für das Profil NACA 0 00 09 - 1,1 30,
   FB 1505/3:   dasselbe für das Profil NACA 0 00 12 - 1,1 30,
   FB 1505/4:   dasselbe für das Profil NACA 0 00 15 - 1,1 30,
   FB 1505/5:   dasselbe für das Profil NACA 0 00 18 - 1,1 30.

   Göthert, B.:   Hochgeschwindigkeitsuntersuchungen an symmetrischen
      Profilen mit verschiedenen Dickenverhältnissen im DVL-Hochgeschwin-
      digkeitswindkanal (2,7 m ∅) und Vergleich mit Messungen in
      anderen Windkanälen. FB 1506.

2. Göthert, B./Richter, G.:   Messungen am Profil NACA 0015-64 im
      Hochgeschwindigkeitswindkanal der DVL (2,7 m ∅), Druckverteilungs-
      auswertung. FB 1247.

   DVL-Industriebericht: Hochgeschwindigkeitsmessungen am Heinkel-
      Profil 0 00 12 - 0,715 36,6 im DVL-Hochgeschwindigkeitswindkanal
      (2,7 m ∅). Editor: B. Göthert. Commissioned by Firma Ernst
      Heinkel Flugzeugwerke G.m.b.H., Rostock.

3. DVL-Industriebericht: Hochgeschwindigkeitsmessungen am Messerschmitt-
      Profile Me 2 35 13 - 1,1 30 im DVL-Hochgeschwindigkeitswindkanal
      (2,7 m ∅). Editor: B. Göthert. Commissioned by Messerschmitt-
      A. G., Augsberg.

4. Ferri, A.:   Alcuni risultati sperimentali riguardanti profili alari
      provati alla galleria ultrasonora di Guidonia.

5. Doetsch, H: Untersuchung der Profilreibe NACA 00 im 5 × 7 m Windkanal
      der DVL. FB 914.

6. Göthert, B.:   Plane and Three Dimensional Flow at High Subsonic
      Speeds. NACA TM 1105, 1946.

7. Winter, H.:   Strömungsvorgänge an Platten und profilierten Körpern
      bei kleinen Spannweiten. Forschung auf dem Gebiete des
      Ingenieurwesens, Bd. 6(1935), Ausg. A, p. 45, figure 16.
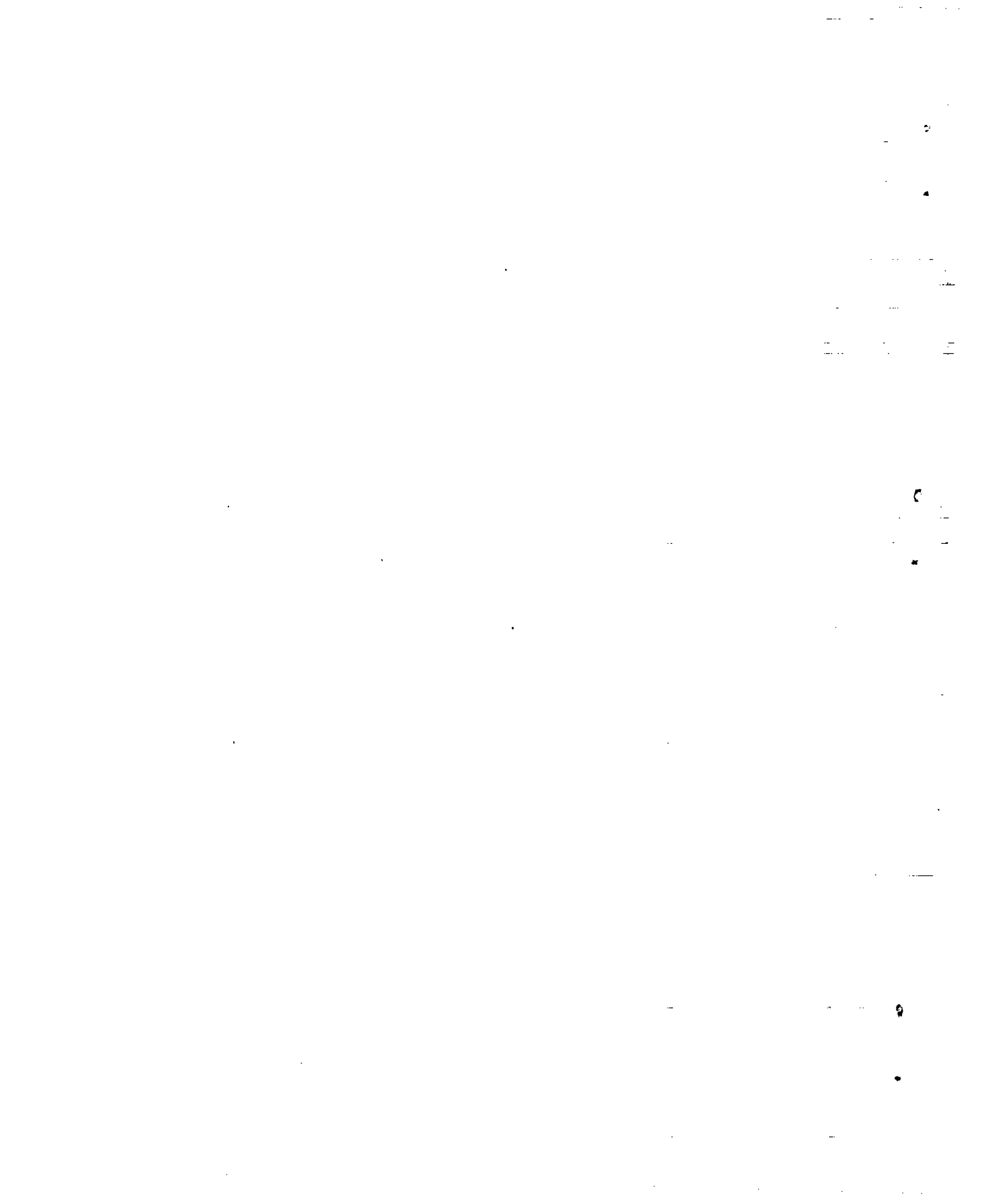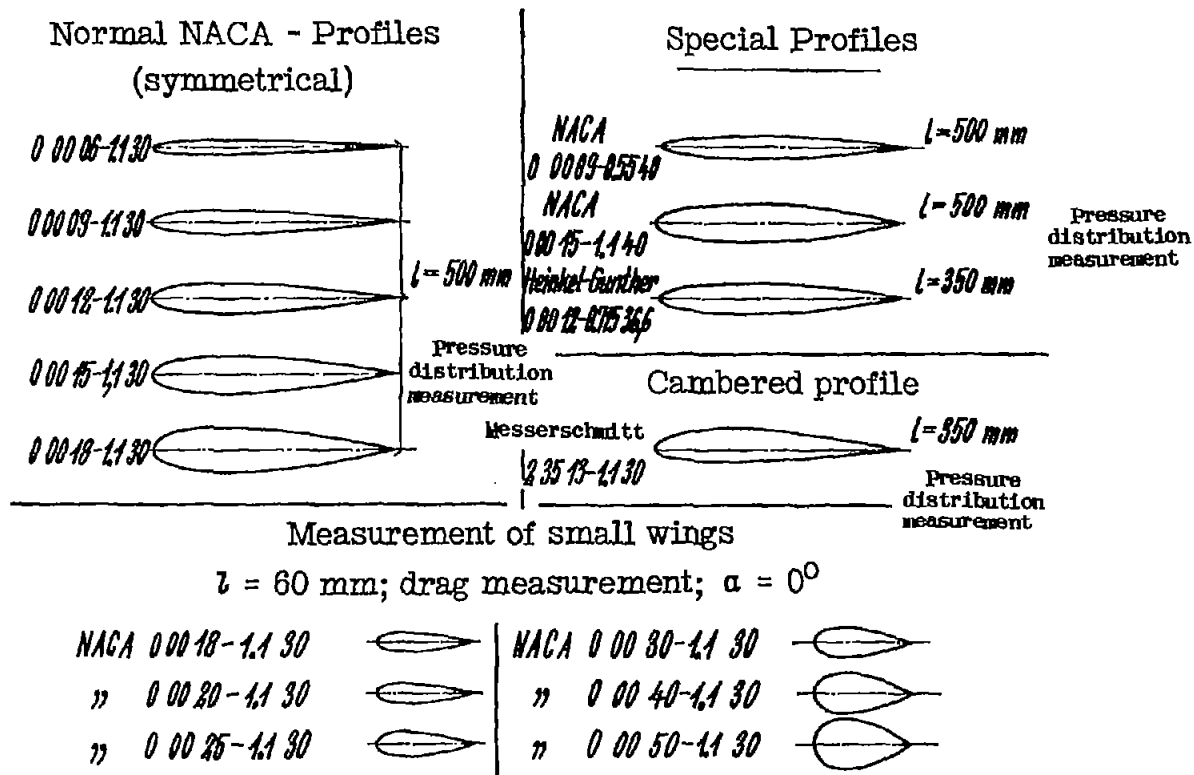
Figure 1.- Profiles tested in the DVL high-speed tunnel.
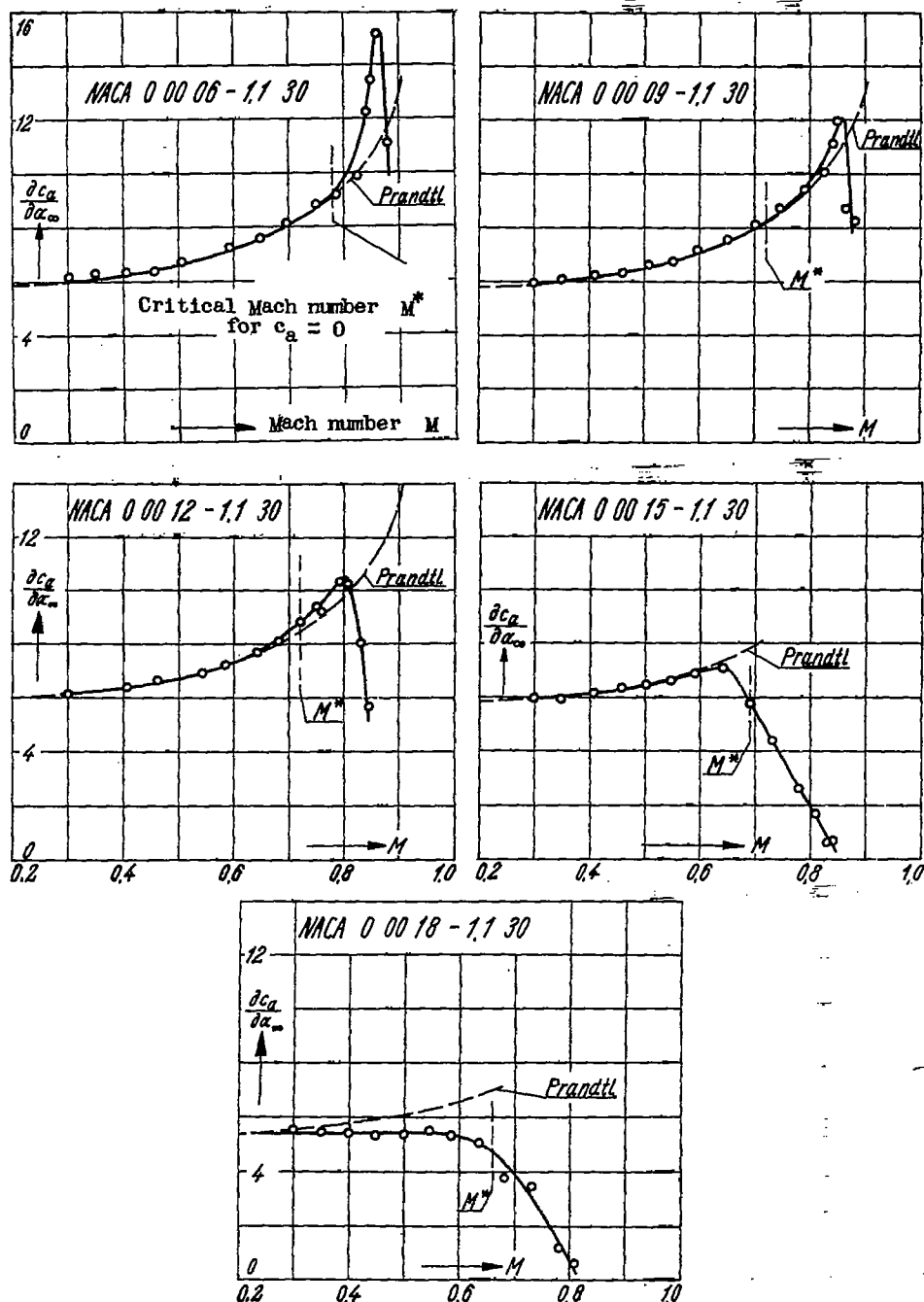
Figure 2.- Lift increase $\partial c_a/\partial \alpha_\infty$ in two-dimensional flow plotted against Mach number for symmetrical NACA airfoils of varying thickness (lift coefficient $c_a \approx 0$).
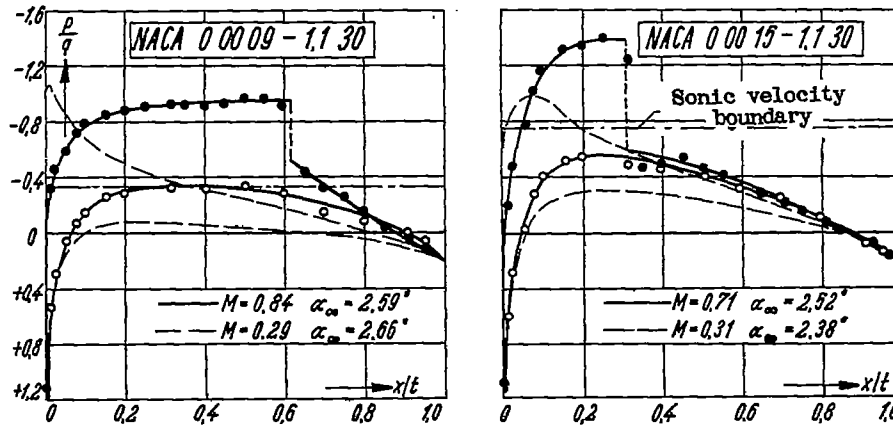
Figure 3.- Pressure distributions of profiles of varying thickness with
expressed compressibility shock on the suction side (pure subsonic flow
yet on the pressure side).
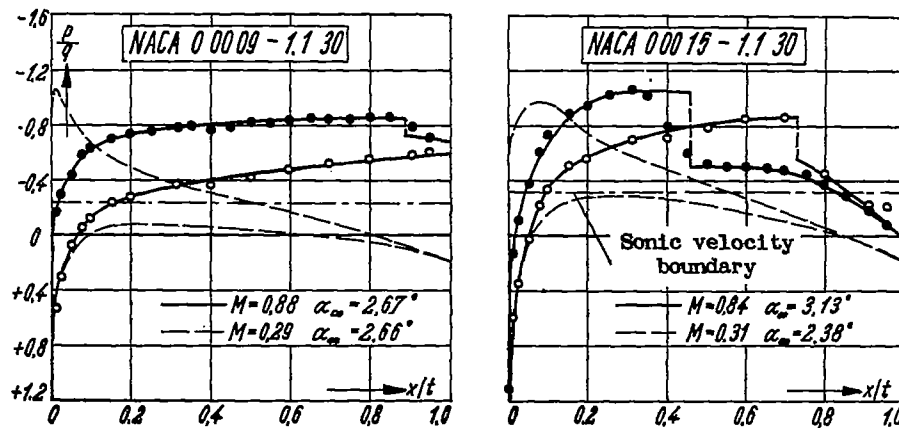
Figure 4.- Pressure distribution with compressibility shocks on suction
and pressure side.
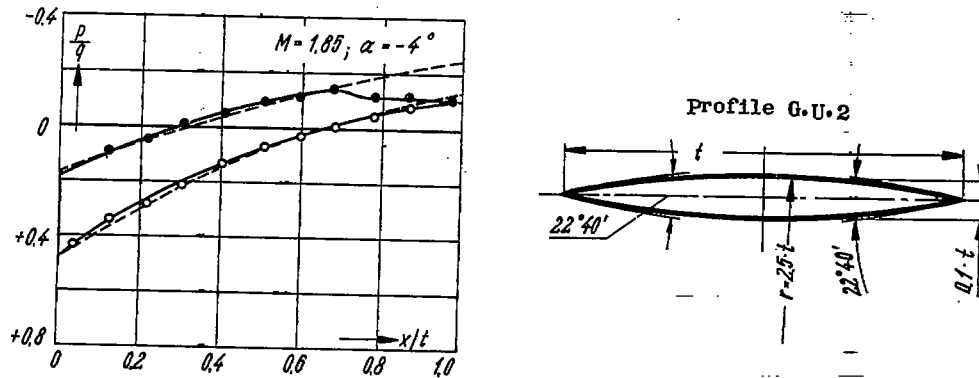
Figure 5.- Pressure distribution at supersonic flow M = 1.85 (according to Ferri).
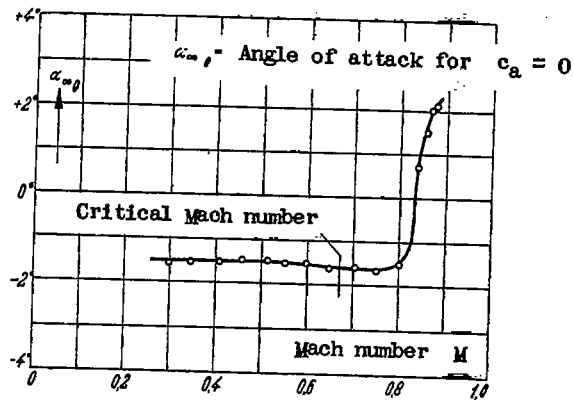
Figure 6.- Angle of attack at zero lift of a cambered profile at high Mach number (profile: Messerschmitt 2 35 13 - 1.1 30).
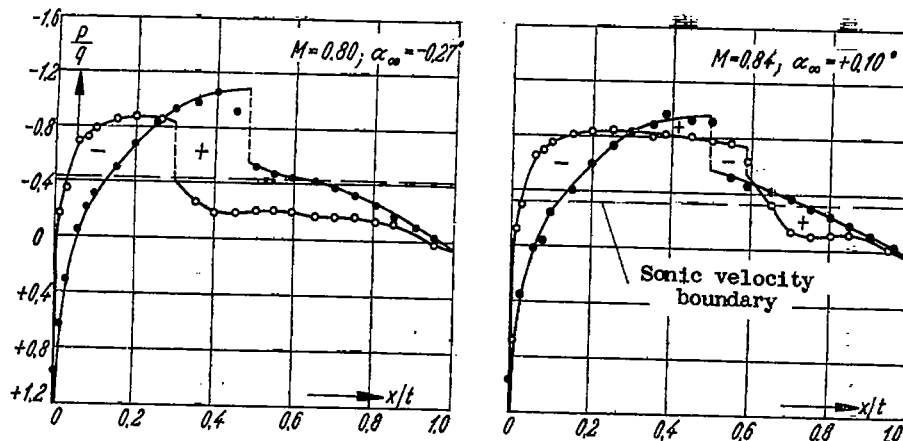
Figure 7.- Pressure distribution on a cambered profile at M = 0.80 and M = 0.84 (angle of attack $\alpha_\infty \approx 0°$) (profile: Messerschmitt 2 35 13 - 1.1 30).
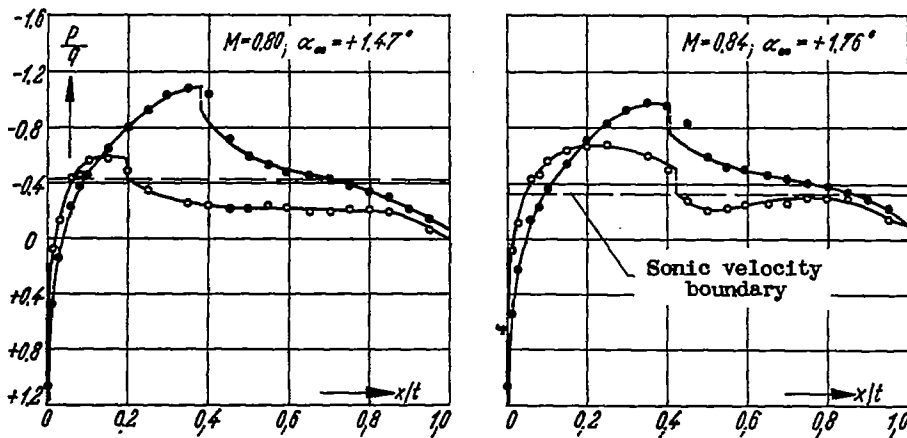
Figure 8.- Pressure distribution on a cambered profile at M = 0.80 and M = 0.84 ($\alpha_\infty \approx 1.6^\circ$). (Profile: Messerschmitt 2 35 13 - 1.1 30)
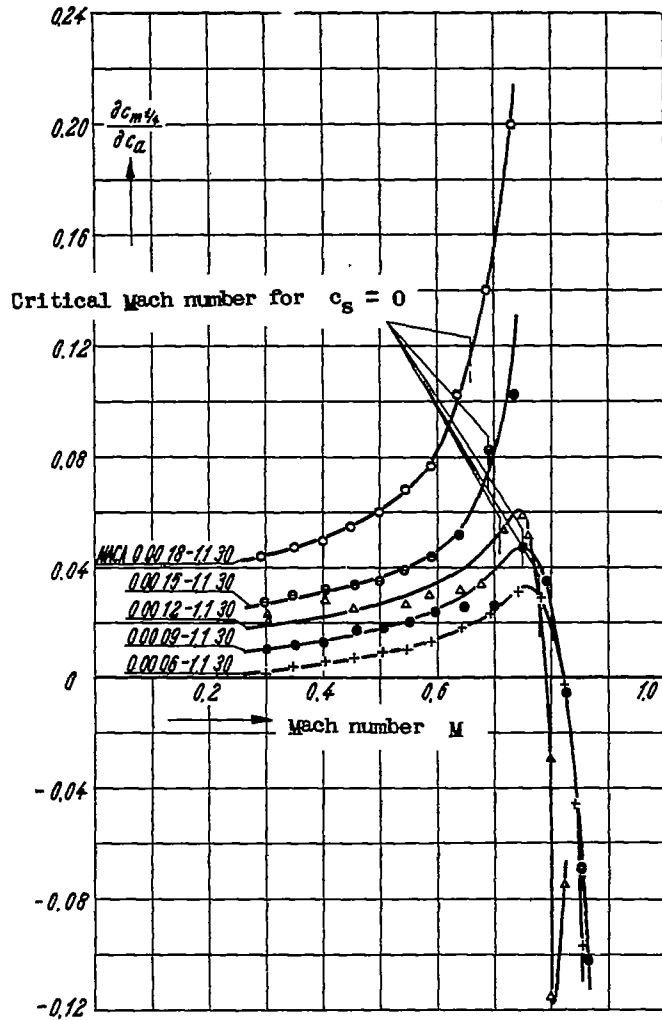
Figure 9.- Neutral stability point position $\partial c_m / \partial c_a$ for various thick symmetrical NACA profiles plotted against Mach number ($c_a \approx 0$).
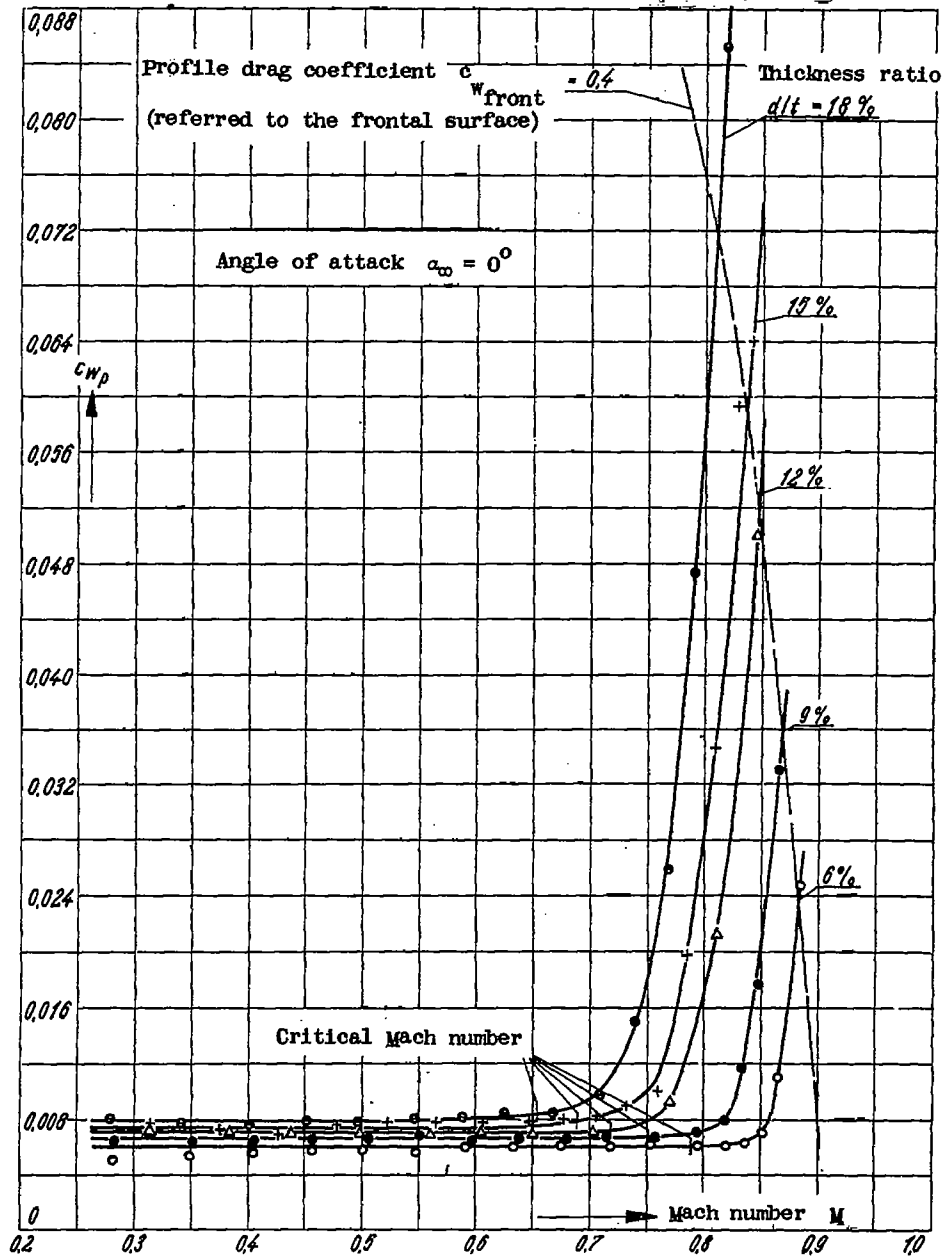
Figure 10.- Profile drag coefficient c_{wp} for various thick symmetrical NACA profiles plotted against Mach number (c_a = 0).
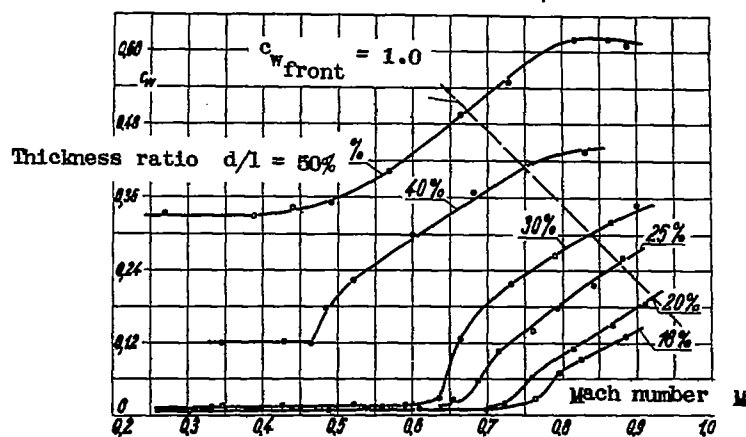
Figure 11.- Drag coefficient c_w at zero lift for thick symmetrical NACA
airfoils plotted against the Mach number (airfoil series 000 d/l - 1.1 30).
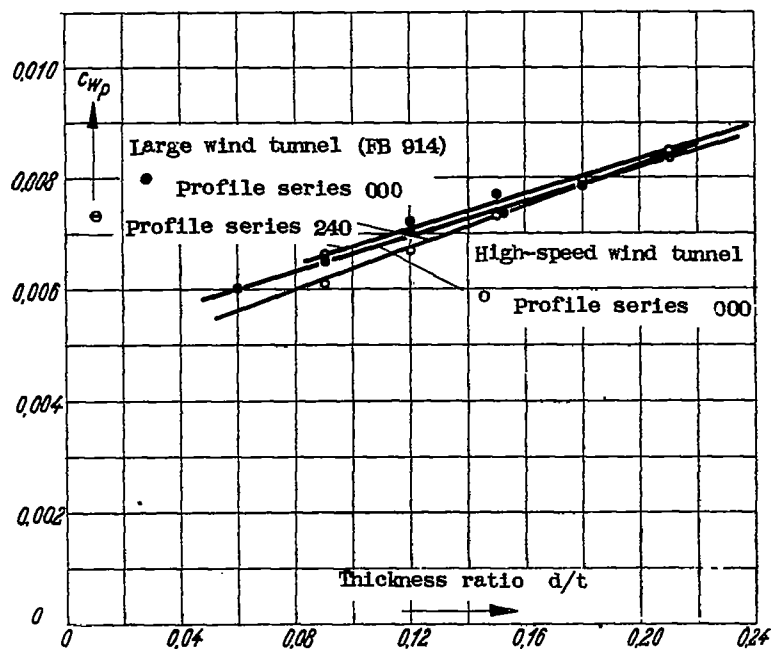
Figure 12.- Profile drag coefficient c_{wp} for profiles of different d/l
(NACA series 000 d/l - 1.1 30 and 2 40 d/l - 1.1 30) according to tests
in the high-speed tunnel and in the large tunnel. Reynolds number in both
cases: R = 2.7 × 10^6; Mach number M ≈ 0.20; lift coefficient c_a = 0.
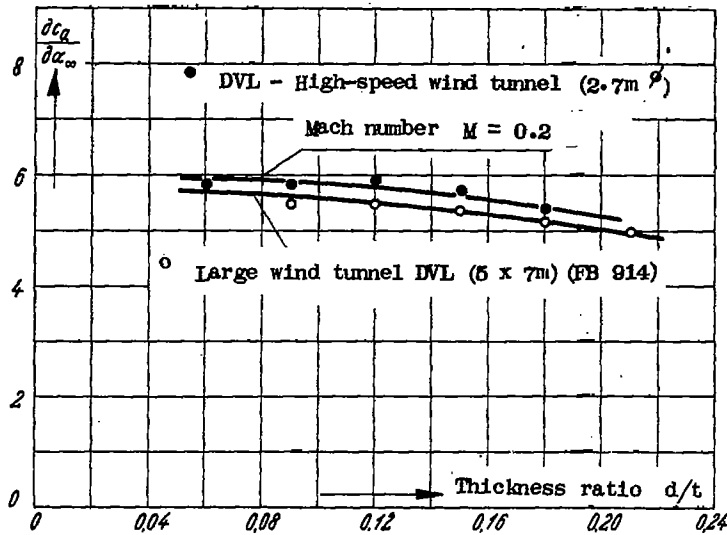
Figure 13.- Lift increase $\partial c_a/\partial \alpha_\infty$ in two-dimensional flow on profiles of different d/l (NACA series 000 d/l - 1.1 30) according to measurements in the high-speed tunnel (pressure distribution measurements) and in the big tunnel (weighing).
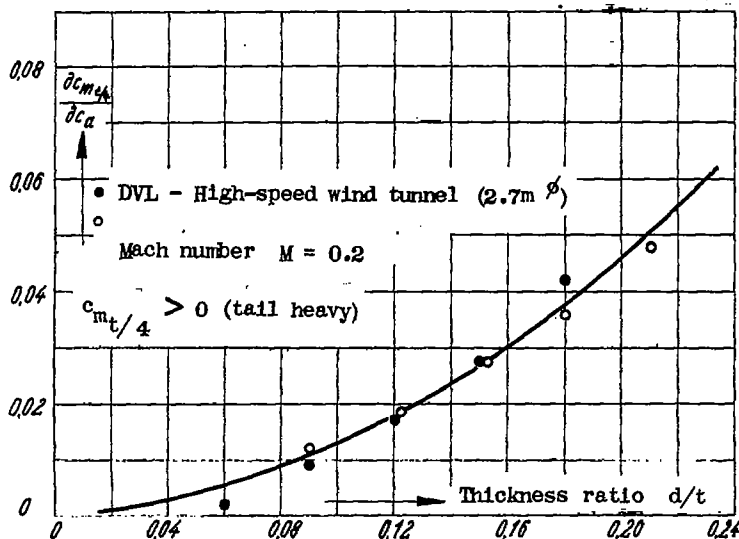
Figure 14.- Neutral stability point position $\partial c_m/\partial c_a$ for profiles of different d/l (NACA series 000 d/l - 1.1 30) according to pressure distribution measurements in the high-speed tunnel and weighing in the big tunnel.
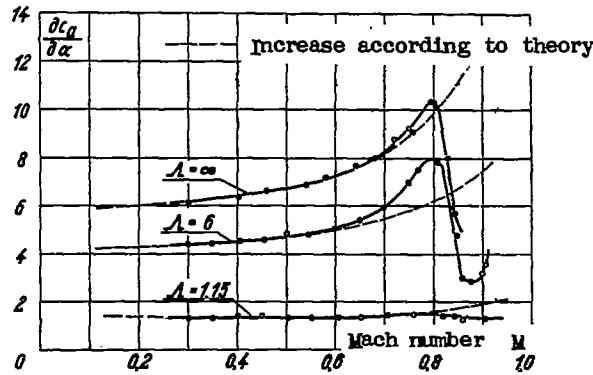
Figure 15.- Effect of aspect ratio Λ on the lift increase $\partial c_a/\partial \alpha$ at high Mach numbers in the zero lift range (NACA series 00012 - 1.1 30).
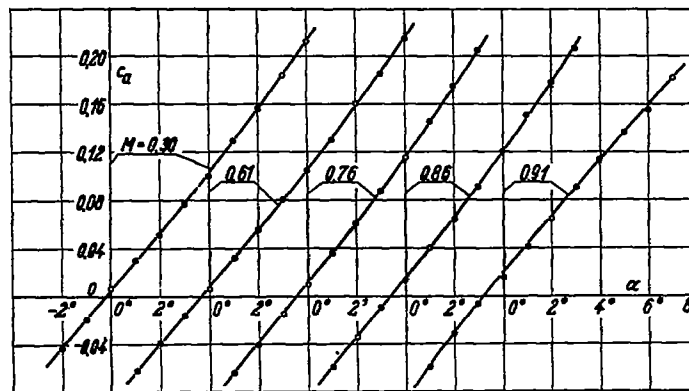
Figure 16.- Lift coefficient c_a plotted against α for a rectangular wing of $\Lambda = 1.15$ and NACA airfoil section 00012 - 1.30 at different Mach numbers M.
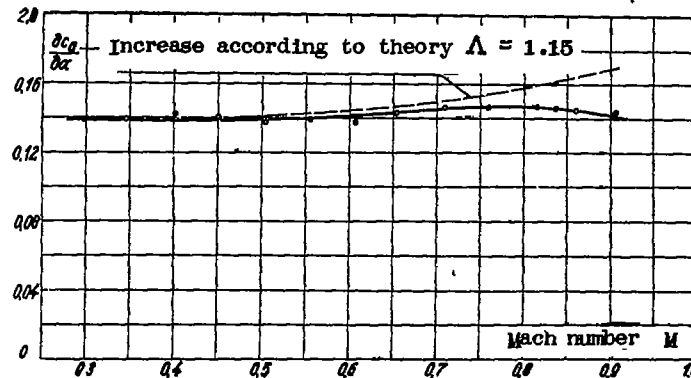
Figure 17.- Lift increase $\partial c_a / \partial \alpha$ of a wing with $\Lambda = 1.15$ and of an airfoil
of the NACA series 00012 - 1.1 30 plotted against the Mach number at
$c_a = 0$.
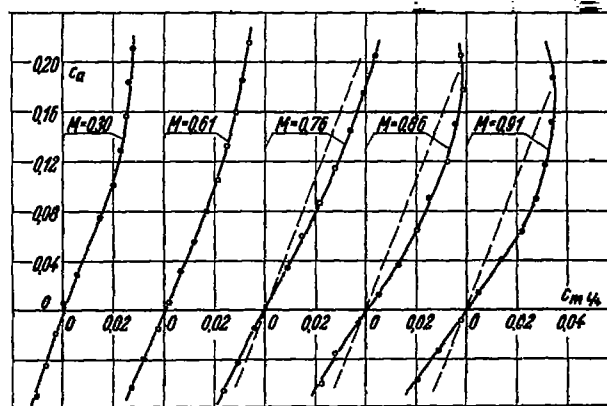
Figure 18.- Moment coefficient $c_m l/4$ plotted against lift coefficient c_a
for a rectangular wing of $\Lambda = 1.15$ and for the profile NACA 00012 -
1.1 30 at different Mach numbers.
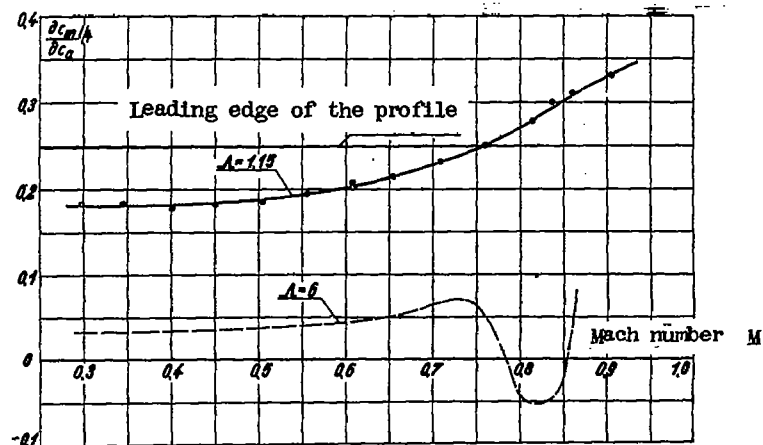
Figure 19.- Neutral stability point $\partial c_m / \partial c_a$ of a wing with $\Lambda = 1.15$ and
profile NACA 00012 - 1.1 30 plotted against Mach number at $c_a = 0$
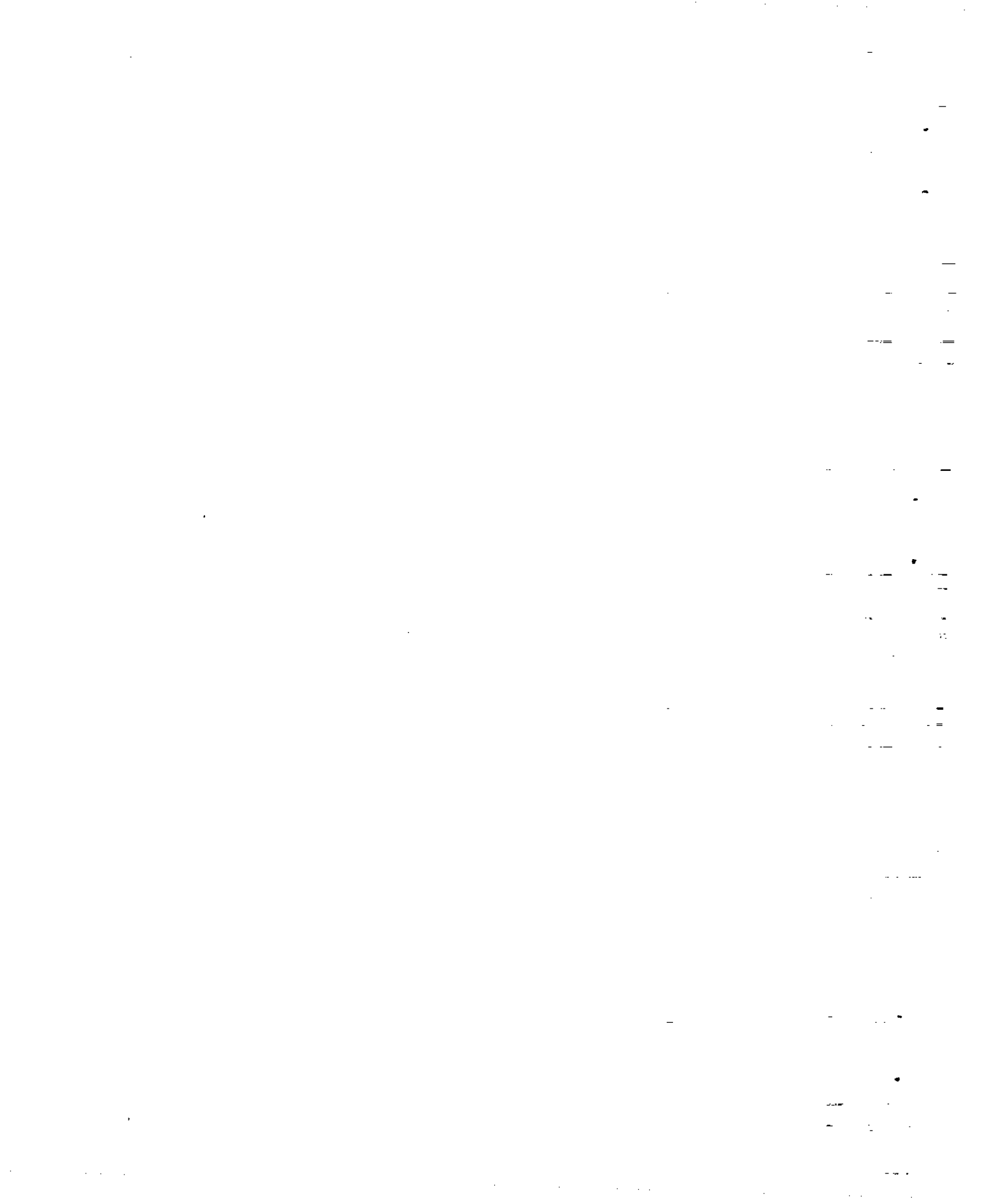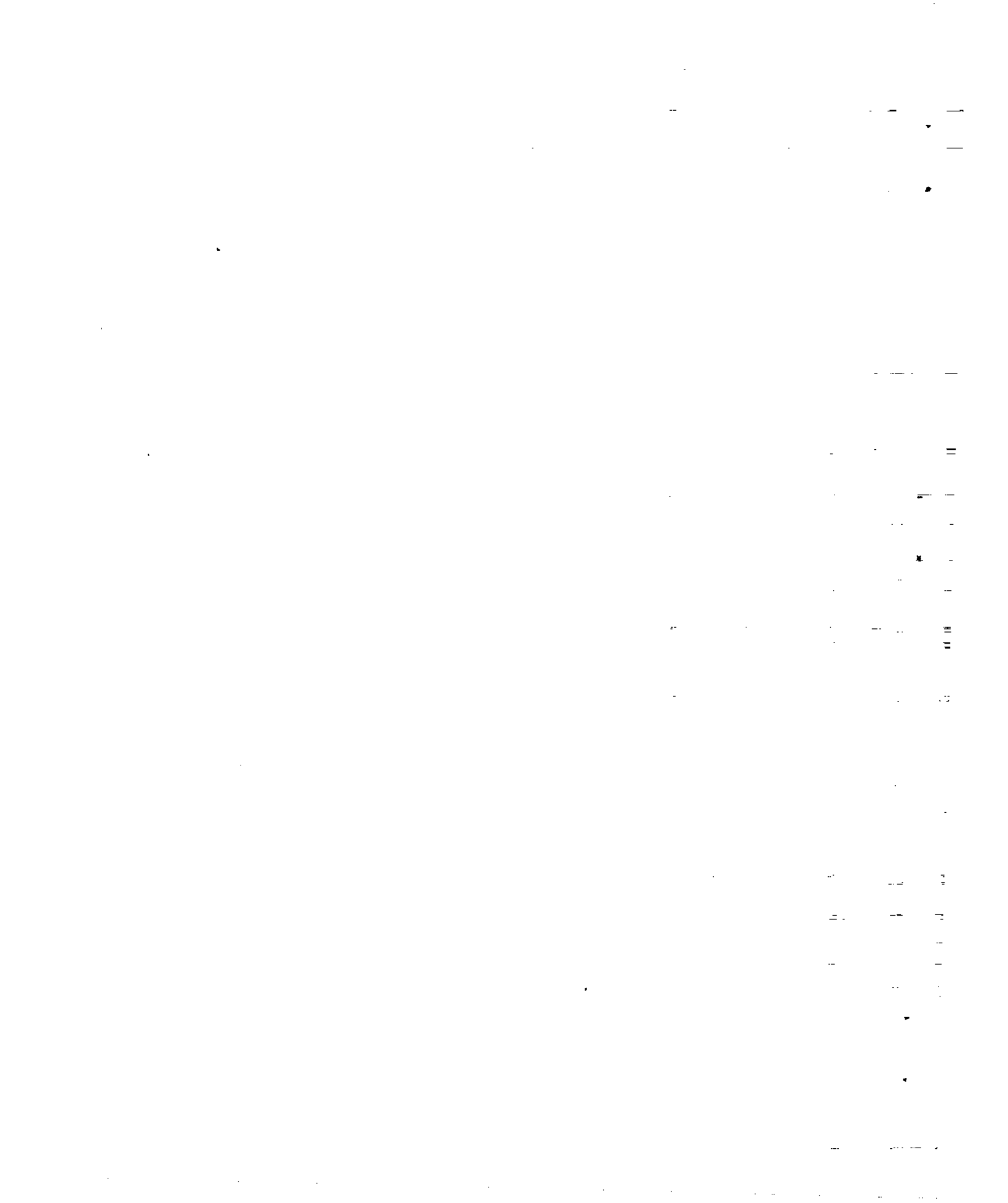($c_m > 0$; tail heavy, referred to $l/4$ line).
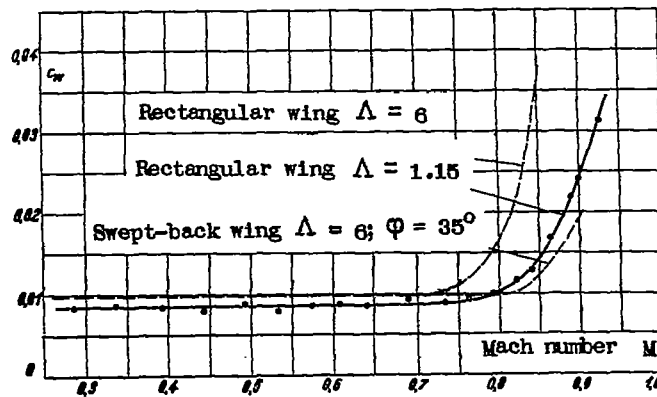
Figure 20.- Drag coefficient c_W at zero lift plotted against Mach number for several model wings of different aspect ratios Λ and angle φ ; profiles of all models measured in flight direction are NACA 00012 - 1.1 30.
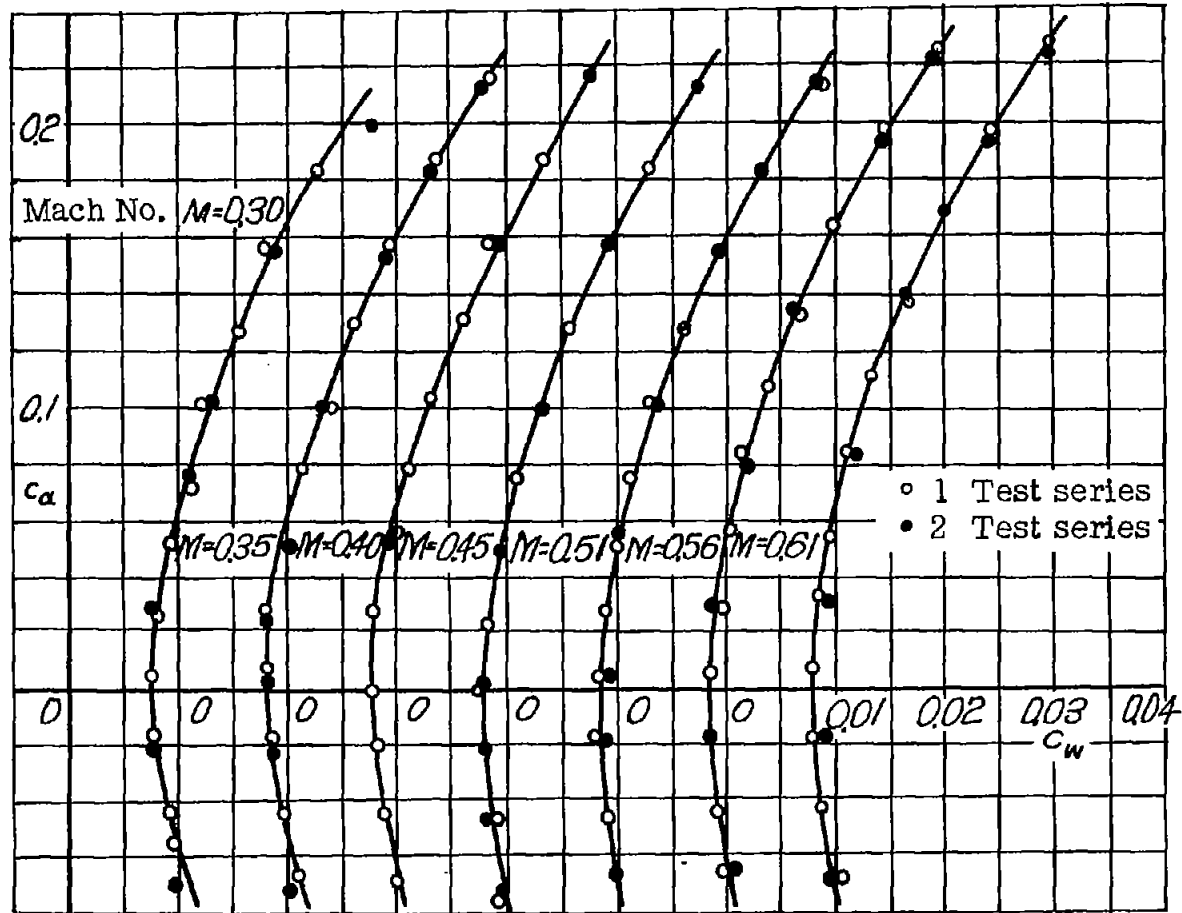
APPENDIX

From Göthert, B.: Hochgeschwindigkeitsmessungen
   an einem Flügel kleiner Streckung.   Zentrale für
   wissenschaftliches Berichtswesen des Luftfahrt-
   forschung des Generalluftzeugmeisters (ZWB)
   Berlin-Adlershof, Forschungsbericht Nr. 1846,
   figures 6 and 7.

High -Speed Measurements
wing with Λ= 1.15 for NACA
profile 00012-1.130
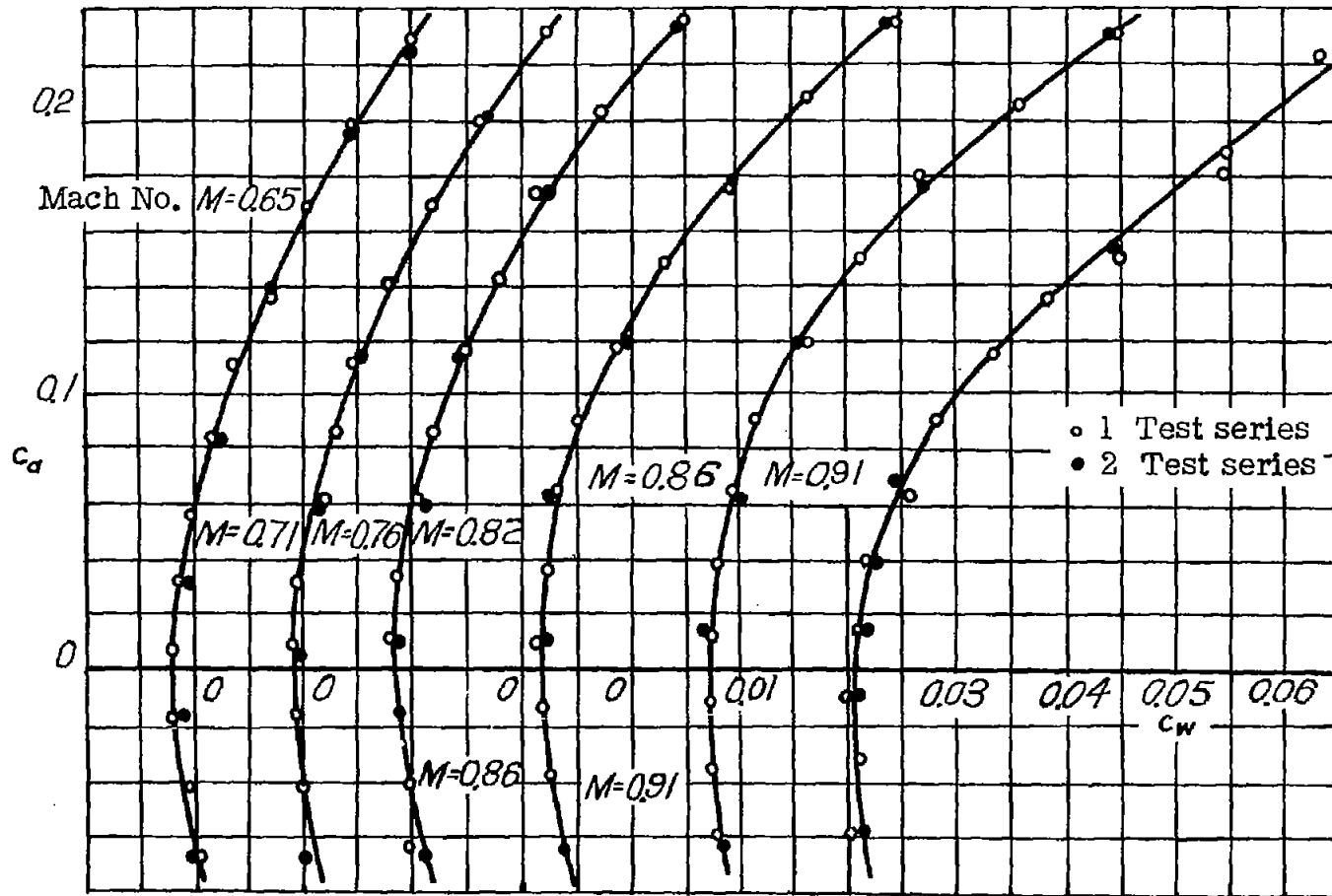
Force
Measurement
Jf 712

Tested
September 21-26, 1942

Figure 6.-   Drag coefficient c_W as a function of lift coefficient c_a at Mach number
M = 0.30 and 0.61.

High - Speed Measurements
wing with $\Lambda = 1.15$ for NACA
profile 00012 - 1.130

Force
Measurement
Jf 712

Figure 7.- Drag coefficient c_w as a function of lift coefficient c_a at Mach number M = 0.65 and 0.91.